RESEARCH ARTICLE | NOVEMBER 07 2023

Influence of incoming turbulence and shear on the flow field and performance of a lab-scale roof-mounted vertical axis wind turbine

Special Collection: Wind Tunnel Research for Renewable Energies

Y. Jooss ⬤ ; R. J. Hearst ⬤ ; T. Bracchi ✉ ⬤

Check for updates

View Online   Export Citation   CrossMark

Influence of incoming turbulence and shear on the flow field and performance of a lab-scale roof-mounted vertical axis wind turbine

Y. Jooss,[a] (iD) R. J. Hearst, (iD) and T. Bracchi[b] (iD)

AFFILIATIONS

Department of Energy and Process Engineering, Norwegian University of Science and technology, Trondheim, Norway

Note: This paper is part of the Special Topic on: Wind Tunnel Research for Renewable Energies.
[a]**Present address:** SINTEF Energy Research, Trondheim, Norway.
[b]**Author to whom correspondence should be addressed:** tania.bracchi@ntnu.no

ABSTRACT

Flow conditions in an urban environment are complex, featuring varying levels of turbulence intensity and shear. The influence of these flow characteristics on the performance of a roof-mounted vertical axis wind turbine of the Savonius (drag) type is investigated at lab scale. Five different inflow conditions are generated with an active grid in a wind tunnel, covering turbulence intensities from 0.9% to 11.5% and relative vertical shear from 0% to 17%. The flow field is captured using particle image velocimetry, and the power output of the turbine is assessed through measurements of the converted power. The set-up consists of two-surface mounted cubes aligned with each other in the main flow direction, spaced apart by two cube heights. The turbine is placed on top of these model buildings at six different streamwise positions along the centerline and at two different heights. It was observed that the turbulence intensity in the inflow has a significant impact on the flow field and also on the power output of the turbine. The increasing turbulence intensity leads to smaller regions of recirculating flow. Thus, the turbine experiences higher flow velocities, which is reflected in the measured power. The influence of shear is comparably small on both the flow field and the turbine performance. The higher of the two turbine positions yields higher power output overall. Furthermore, it was shown that the impact of the turbine on the flow field is significant for all inflow conditions and can vary substantially depending on the inflow.

I. INTRODUCTION

One of the United Nation's sustainable development goals is to provide access to sustainable and modern energy for everyone.[1] Urban wind energy can be classified as such a source of modern and renewable energy. However, it has received relatively little attention, compared to wind farms installed in open areas, largely due to the complex wind resources caused by the presence of the built environment.[2] In such an environment, the atmospheric boundary layer is altered by the presence of the buildings,[3] and we then refer to it as an urban canopy layer from the ground up to about building height and an urban boundary layer above.[4] The urban canopy layer is dominated by microscale effects[5] with the flow being primarily dependent on the geometry of the local surroundings.[6] This leads to large regions of low velocities, which is why most wind turbines in urban environments are placed above that, in the roughness sublayer.[3] The roughness sublayer extends from the building roofs to roughly 2–5 building heights.[3,7]

Here, the flow is still mainly governed by individual roughness elements,[6] such as buildings, but some homogenization has occurred. This is the region examined in this study.

The velocity in the atmospheric boundary layer and in large parts of the urban boundary layer is typically vertically sheared and often assumed to follow a logarithmic profile, or a power law. However, Wagner et al.[8] showed that this is a notable simplification. They classified the atmospheric boundary layer into 173 different wind profiles through 2340 independent field measurements from 40 to 160 m above the ground. Large variations in the vertical shear were found between approximately $\Delta U(z)/U_\infty = 6\%$ and 63%, where ΔU is the velocity difference from bottom (40 m) to top (160 m) in the examined region with reference velocity $U_\infty = 7$ m/s at 80 m above the ground. Only rarely the profiles follow a logarithmic profile or a power law. The turbulence intensity, defined as the ratio between velocity fluctuations and the mean velocity u'/U, in the atmospheric boundary layer

can reach up to 40% with typical values situated around 5%–15%.[9] In the roughness sublayer, the turbulence is subject to local variations. Roth[10] reported turbulence intensities measured in the roughness sublayer between 20% and 40%. This creates a complex flow problem with variably sheared flow and varying high turbulence intensities interacting with individual roughness elements such as buildings. This is schematically depicted in Fig. 1.

Placing a wind turbine in such an environment is non-trivial. Having a good understanding of the flow field is important, as the available power of a wind turbine scales with the velocity cubed, $P_a = \frac{1}{2}\rho U^3 A$, with the rotor swept area A and the air density ρ. Small differences in velocity can, thus, have a large impact on the power output of a turbine. This becomes more complicated when taking turbulent fluctuations, wind shear, and directional shear into consideration.[11] More insight into the siting of a roof-mounted wind turbine has been gained, through studies assessing the flow around model buildings, e.g., by Mertens,[12] Ledo et al.,[13] and Abohela et al.[14] However, these relied on modeling the turbulence in their simulations. Experimental studies are needed to complement the simulations[2] such as by Al-Quraan et al.,[15] Sarkic Glumac et al.,[16] and Vita et al.[17] Furthermore, it has been demonstrated that the interaction of a wind turbine with the flow in such an environment is complex and not easily predictable.[18] It extends beyond blockage effects documented for wind turbines generally,[19] as well as in complex terrain, such as hills.[20] Thus, a wind turbine is included in the present study. To enable an experiment incorporating both buildings and a wind turbine in controlled flow conditions, the set-up is scaled down by several orders of magnitude. This is common practice in lab-scale studies of wind turbines.[21–30] While not achieving necessarily dynamic similarity, these studies are meaningful in identifying the underlying trends of a problem with good control of the examined parameters.

A simple drag-driven Savonius turbine with a vertical axis of rotation is employed in the present study. Vertical axis wind turbines (VAWTs) have received increased attention of late[31–36] and are often employed in environments where horizontal axis wind turbines (HAWTs) experience difficulties.[37] Their omnidirectionality makes them a good fit for the urban environment.[35,38,39] Pagnini et al.[40] found increased robustness to gusts and high wind velocities compared to HAWTs. VAWTs to mount on roofs can be purchased in sizes approximately between 1 and 6 m from various industrial manufacturers, leading to typical turbines to build size ratios of 0.08–1.44 for one to three storey-buildings.

Buildings are often modeled as surface mounted cubes in experimental and numerical studies.[3,14,18,41,42] This approach is also used in the present study with two-surface mounted cubes placed in line with each other in the flow direction with a distance of two cube heights (h).
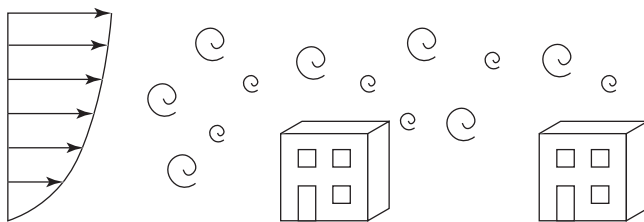

FIG. 1. Schematic of the flow that buildings encounter in the urban environment.

in between. The flow on this configuration has been studied by Martinuzzi and Havel[43,44] and Jooss et al.[18] for low turbulence intensities and uniform inflows. To account for the above described complexity that is presented by an urban flow field, in the present study, the turbulence intensity and vertical shear are varied in the inflow. The influence of turbulence intensity on a single cube has been documented by Yakhot et al.[45] and Hearst et al.[46] Here, we will examine the influence of five different inflow conditions on the flow field around two cubes, as well as on the performance of a roof-mounted VAWT at six streamwise positions and two heights, yielding a total of 60 cases.

II. EXPERIMENTAL PROCEDURE

The basic experimental set-up, depicted in Figs. 2(a) and 2(b), consists of two $h = 100$ mm cubes mounted to a circular acrylic plate of $d = 14h$ and a thickness of $0.1h$ with a 15° sharp leading edge. The cubes are placed in line with each other with respect to the flow with a spacing of $s = 2h$ and a distance of $5h$ to the leading and trailing edge. The center of the upstream cube is denoted as $x = 0$ with $z = 0$ at the artificial floor the plate provides. The two cubes resemble one building relatively unaffected by its surroundings (the upstream cube) and one very much affected by a neighboring building (the downstream cube). The spacing was carefully chosen based on a study by Martinuzzi and Havel,[43] which showed that this is representative for $1.4 \leqslant s/h \leqslant 3.5$. A VAWT is placed at various positions on top of the two cubes. Six streamwise positions, as illustrated in Fig. 2(c), and two different heights, $0.08h$ and $0.16h$ between the cube and the bottom of the turbine, are examined, resulting in a total of 12 positions. They are labeled L and H for the low and high turbine positions and numbered 1–6 from most upstream to most downstream (1–3 on the upstream cube and 4–6 on the downstream cube), e.g., L1 for the low turbine at the most upstream position. The VAWT is a generic two-bucket Savonius (drag) type turbine designed based on the work of Alexander and Holownia[47] and Akwa et al.[48] Figure 2(d) shows the cross section of the blades. It consists of two semi circles with a diameter d_T of $0.4h$ and a blade height h_T of $0.3h$ with an overlap of $0.05h$ between the blades to decrease the starting torque.[49] The same turbine has been used in Jooss et al.[18] The size ratio between turbine and building represents a typical VAWT installation for one to three storey-houses and buildings.[18]

To evaluate the turbine performance at the different positions, the converted power, P_c, is measured as described in Jooss et al.[18] For this, the turbine is connected to a brushed DC motor (12G88 Athlonix) functioning as a generator. The rotational velocity of the turbine Ω_T is tracked with a reflective object sensor (OPB705WZ). Bastankhah and Porté-Agel[50] showed that P_c provides a good approximation of the mechanical power of the turbine, P_m, as it only differs by the friction losses, P_f, which can be approximated with knowledge of the motor properties. The rotational velocity of the turbine is controlled through a high frequency variable switch (RF540NPbF) connected to an Arduino Uno. A similar method was used in recent studies by Gambuzza and Ganapathisubramani[30] and Jooss et al.[18]

The experiments were conducted in the large scale wind tunnel at the Norwegian University of Science and Technology. This is a closed loop tunnel with a test section of $2.71 \times 1.80 \times 11.15$ m³ (width × height × length). The flat plate is elevated 0.60 m from the wind tunnel floor with the cubes centered in the transverse direction, such that the flow around the cubes is unaffected by the wind tunnel floor and wall boundary layers. A schematic of the set-up is shown in Fig. 2(a).
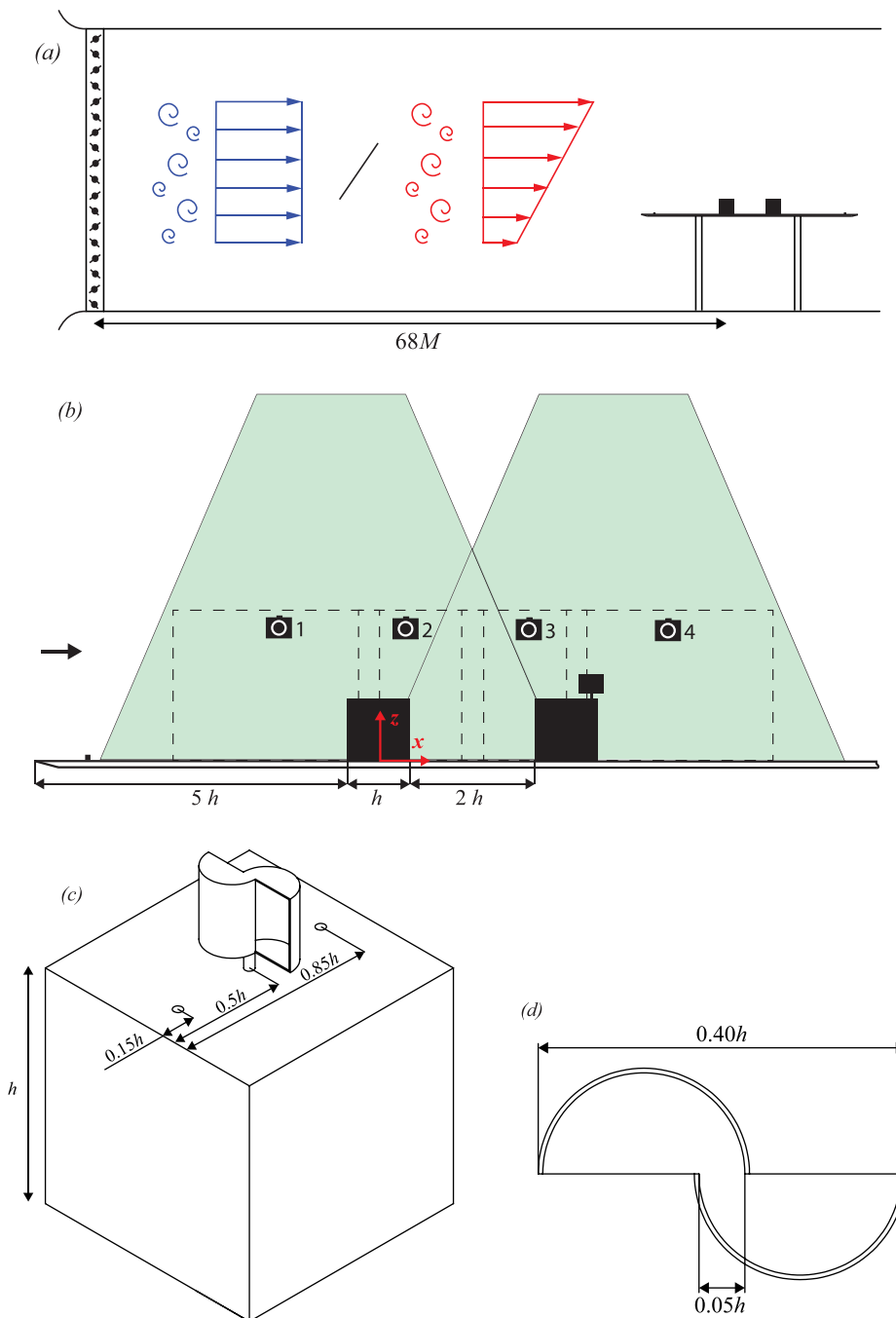
FIG. 2. Experimental set-up: (a) Wind tunnel schematic with active grid and cube set-up. Note, the distance from the active grid to the set-up is not to scale. (b) PIV set-up with two synchronized lasers and four cameras to capture the flow field. (c) Savonius turbine at three positions on the roof of a cube.[18] (d) Blade cross section of the Savonius turbine.[18]

The overall blockage of the model is below 3.8% and can, thus, be considered negligible.[51] An active grid (Fig. 3) at the inlet of the test section is used to tailor the inflow, generating different levels of inflow turbulence intensity and vertical shear. The grid consists of a total of 90 individually controlled stepper motors, 18 on each side for the horizontal rods, and 27 on the top and bottom for the vertical rods. Each motor controls one rod that extends from the edge of the test section to the central vertical or horizontal support structure where it is connected to a bearing. In addition, there are two more vertical support structures with bearings, one on each side of the center. The rods are equipped with square-shaped wings with a 97.6 mm diagonal. The mesh length M of the grid is the distance between the rods, which is 100 mm. Two principal actuation modes were used with the actuation parameters reported in Table I. For case A and case B, all the
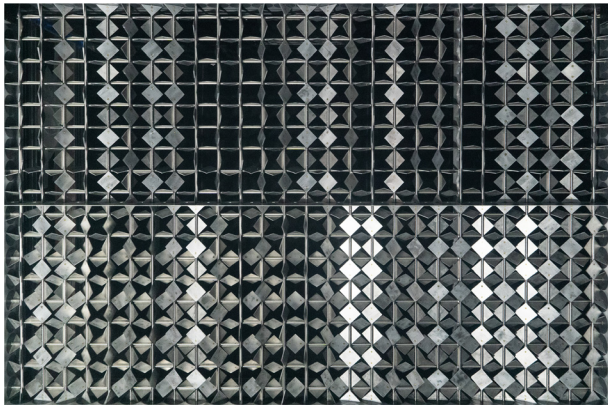
FIG. 3. Active grid in mode C. Note the decreasing blockage from bottom to top to create vertical shear.

wings were actuated fully randomly. That is, the rotational velocity, acceleration, and update frequency are randomly varied within a set range.[52] This creates a uniform velocity profile. It was shown that the variation of the mean rotational velocity directly impacts the turbulence intensity in the freestream with lower Ω_G leading to higher u'_∞/U_∞.[52–54] This is utilized here to create two different levels of turbulence intensity for cases A and B. For case C, only the vertical wings were actuated fully randomly. For A and C, the mean rotational velocity Ω_G was set to 7 Hz and varied by $\pm\omega_G = 3.5$ Hz with a top-hat distribution. Case B has a distribution of 2 Hz $\pm$ 1 Hz. To create shear in the vertical direction, the horizontal wings for C and D oscillate around $\theta = 0°$ with increasing $\pm\theta$ from bottom to top.[55] To limit the turbulence production in the wind tunnel due to $\partial U/\partial z$, only the center eight wings were used to create shear with the top five wings remaining still at $\theta = 0°$, and the bottom five wings oscillating at the maximum angle $\theta_{G,\max}$. A larger $\theta_{G,\max}$ yields a higher velocity gradient;[55] thus, it was varied between 45° for case C and 60° for case D to create different levels of shear. To avoid the imprint of the flapping frequency on the spectral distribution of energy, the flapping frequency was varied randomly for both cases with $F_G \pm f_g = 3.5$ Hz ± 1.5 Hz.

To examine the impact of these different inflow conditions on the flow, the velocity fields around the cubes were measured. They were acquired using planar particle image velocimetry (PIV) along the center xz-plane of the set-up as schematically shown in Fig. 2(b). Two synchronized dual-pulse Litron Nd-YAG laser (Nano L200–15 PIV), with

a wavelength of 532 nm and a maximum power of 200 mJ, were used as light sources. The flow was seeded with 1 μm DEHS particles created by a LaVision Aerosol Generator PivPart45-M. A total of four cameras were used simultaneously to capture the flow: two LaVision Imager LX 16 mega-pixel cameras with Nikon 200 mm lenses in the center flanked by two LaVision Imager MX 25 cameras with Zeiss 100 mm lenses up- and downstream. This gave a large total field of view of 980×240 mm² (width $\times$ height). Vector fields were calculated from the particle images in Davis 8.4.0. A decreasing window size of 96×96 on the initial pass, and 48×48 on the final pass were used. A 50% overlap on the final pass yielded a vector spacing of 1.5 mm. To obtain information on the energy spectra and integral length scales, the PIV measurements were supplemented by single point hot-wire measurements of the background flows. A Dantec 55P11 single hot-wire probe was used together with a Dantec StreamLine Pro anemometer operated at an overheat ratio of 1.8. The hot-wire data were acquired at a sampling frequency of 75 kHz and low pass filtered at 30 kHz, both well above the Kolmogorov frequency of $\sim$10 kHz.

III. FLOW CHARACTERIZATION
A. Inflow

The influence of five different inflow conditions on the performance of a roof-mounted VAWT is examined in the present study. Specifically, the influence of freestream turbulence intensity and shear are investigated. Four of the inflow conditions are generated using the above described active grid, with a clean configuration without a grid serving as a low turbulence intensity reference case in addition. The actuation parameters, together with the resulting flow parameters, are listed in Table I. To evaluate the inflow conditions, PIV and hot wire measurements were conducted above the plate, without the cubes or turbine present. The different inflow cases were compared at the position of the windward face of the upstream cube, at $x/h = -0.5$, with $z/h = 1$ serving as the reference height. The velocity was fixed to $U_\infty = 10.7 \pm 0.2$ m/s, giving Reynolds numbers of $Re_h = U_\infty h/\nu \approx 67\,000$ and $Re_{d_T} = U_\infty d_T/\nu \approx 27\,000$, based on the cube height and the turbine diameter, respectively, with the kinematic viscosity ν. The Reynolds numbers are of course low compared to those in the urban environment. However, for flow around a single cube with uniform inflow, the Reynolds number independence for the mean quantities has been found for $Re_h > 30\,000$ in Refs. 56 and 57. For a two-cube set-up, the Reynolds number independence was shown in Martinuzzi and Havel[43] between $Re_h = 12\,000$ and $40\,000$. This indicates that the flow patterns observed at lab scale for the cubes are representative. While the turbine performance is affected by the low

TABLE I. Active grid configurations and flow parameters of the five different inflows.

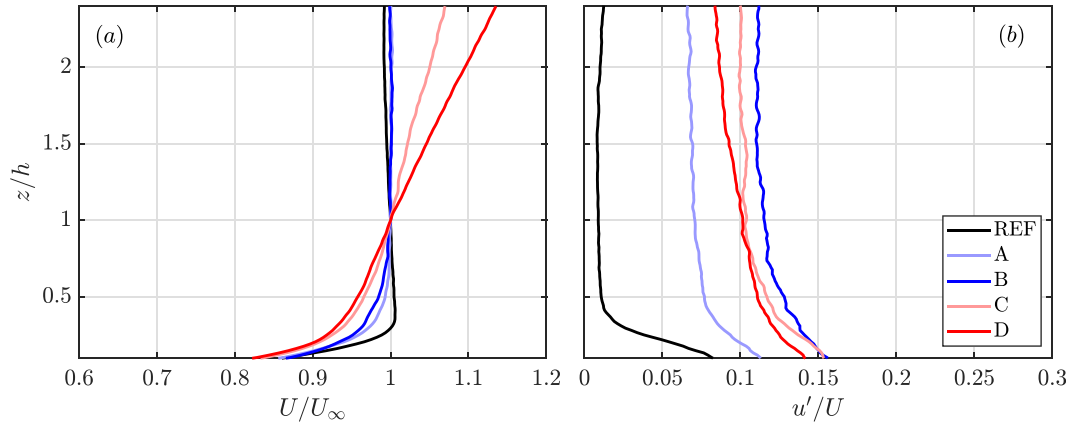| Case | Horizontal wings | | | Vertical wings | Flow | | | | | |
	$\Omega_G \pm \omega_G$ (Hz)	$F_G \pm f_g$ (Hz)	$\pm\theta_{G,\max}$ (deg)	$\Omega_G \pm \omega_G$ (Hz)	U_∞ (m/s)	u'_∞/U_∞ (%)	$\Delta U(z)/U_\infty$ (%)	$L_{u,\infty}/h$	u'_∞/w'_∞	Color
REF	$\cdots$	$\cdots$	$\cdots$	$\cdots$	10.8	0.9	$\sim$0	0.6	0.97	■
A	7 ± 3.5	$\cdots$	$\cdots$	7 ± 3.5	10.9	7.1	0	2.0	1.41	■
B	2 ± 1	$\cdots$	$\cdots$	2 ± 1	10.9	11.5	0	2.5	1.44	■
C	$\cdots$	3.5 ± 1.5	45	7 ± 3.5	10.7	10.4	9	2.9	1.55	■
D	$\cdots$	3.5 ± 1.5	60	$\cdots$	10.5	10.2	17	3.0	1.89	■

09 November 2023 09:46:12

FIG. 4. Background profiles of (a) the streamwise velocity normalized by U_∞ and (b) the streamwise turbulence intensity. Note, these profiles are averaged over five vectors in the streamwise direction at the position of the leading edge of the first cube, $x/h = -0.5$ and $z/h = 1$.

Reynolds number,[48] the goal of this study is not to maximize the turbine performance, but rather to compare the energy extraction at different positions; thus, the absolute values of power extraction are not critical here. The streamwise turbulence intensity u'_∞/U_∞ in the free stream is varied from 0.9% for case REF to 7.1% for case A and 11.5% for case B. This is in line with typically reported values in the atmospheric boundary layer[9] with peak values in the roughness sublayer reaching up to fourfold of this. All three cases have a vertically uniform velocity profile outside of the thin boundary layer. This is deliberately varied for cases C and D, which have increasing shear $\Delta U(z)/U_\infty$ of 9% and 17%, that is, the velocity difference ΔU from just outside the boundary layer to the top of examined region, where the shear is linear, normalized by U_∞. This is comparable to the typical levels of shear reported by Wagner *et al.*[8] for their atmospheric measurements with maximum levels reaching almost fourfold of this. u'_∞/U_∞ was approximately matched among cases B, C, and D to examine the influence of the shear. The velocity profiles for all cases, normalized by U_∞, are displayed in Fig. 4(a). The turbulence intensity is approximately constant outside the boundary layer for all cases. u'/U profiles are shown in Fig. 4(b). The integral length scale is estimated from the integration to the first zero crossing of the autocorrelation of the hot-wire measurements and normalized by h. A high-pass filter at 0.4 Hz is used to counteract the effect of non-stationary low frequencies on the calculation of $L_{u,\infty}$. Decaying autocorrelation functions and clean zero-crossings have been observed for all presented cases. $L_{u,\infty}/h$ increases with turbulence intensity from 0.6 for case REF up to 2.5 for case B. This trend is in agreement with active grid studies by Hearst and Lavoie[52] and Mydlarski and Warhaft.[53] The relatively slow flapping of the horizontal wings in cases C and D increases $L_{u,\infty}/h$ slightly further. The isotropy ratios u'_∞/w'_∞ have been calculated from the background PIV measurements. Measurements in the empty tunnel showed $1 \leqslant u'_\infty/w'_\infty \leqslant 1.1$. The presence of the plate leads to an increase in u'_∞/w'_∞ for the turbulent cases (see Table I). The isotropy values for cases A and B still remain in line with previous active grid studies.[58,59] The flapping cases (C and D) show relatively high anisotropy, due to the slow flapping motion. This is in agreement with similar shear flows.[60] All values are listed in Table I. The energy spectra, normalized by the Kolmogorov length scale η and ν, are plotted

against the product of the wave number κ and η in Fig. 5. A clear distinction between the low turbulence case REF and the four active grid cases is apparent in the extent of the inertial sub-range. Case A shows a slightly lower total energy compared to cases B–D, which collapse reasonably well through all scales. There is no imprint of the actuation protocol at distinct frequencies visible in the spectrum for any case, suggesting that the turbulent structures at this point are relatively unaffected by the way they were generated.

B. Flow field

To understand the conditions the turbine is exposed to, the flow field around the cubes is analyzed for the different inflow cases. To normalize all velocities in the following analysis, the velocity far upstream of the cubes at $x/h = -3.5$ cube height $z/h = 1$ is used as a reference velocity U_0. The flow here is unaffected by the varying turbine position. For REF, the total scatter of U_0 between all positions, including the case without a turbine, is less than 0.4% with no apparent trend. The streamwise velocity at this position is slightly affected by the presence of the cubes, which are present for all examined cases
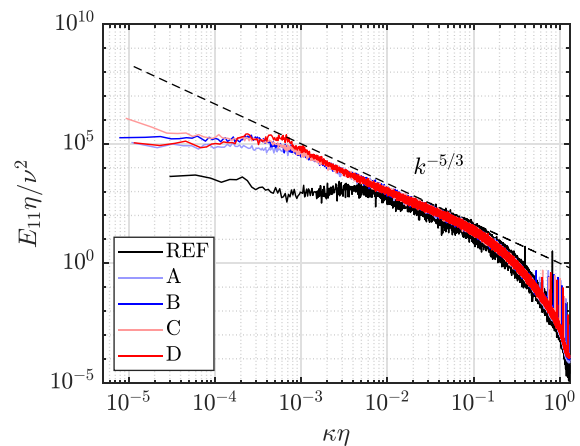

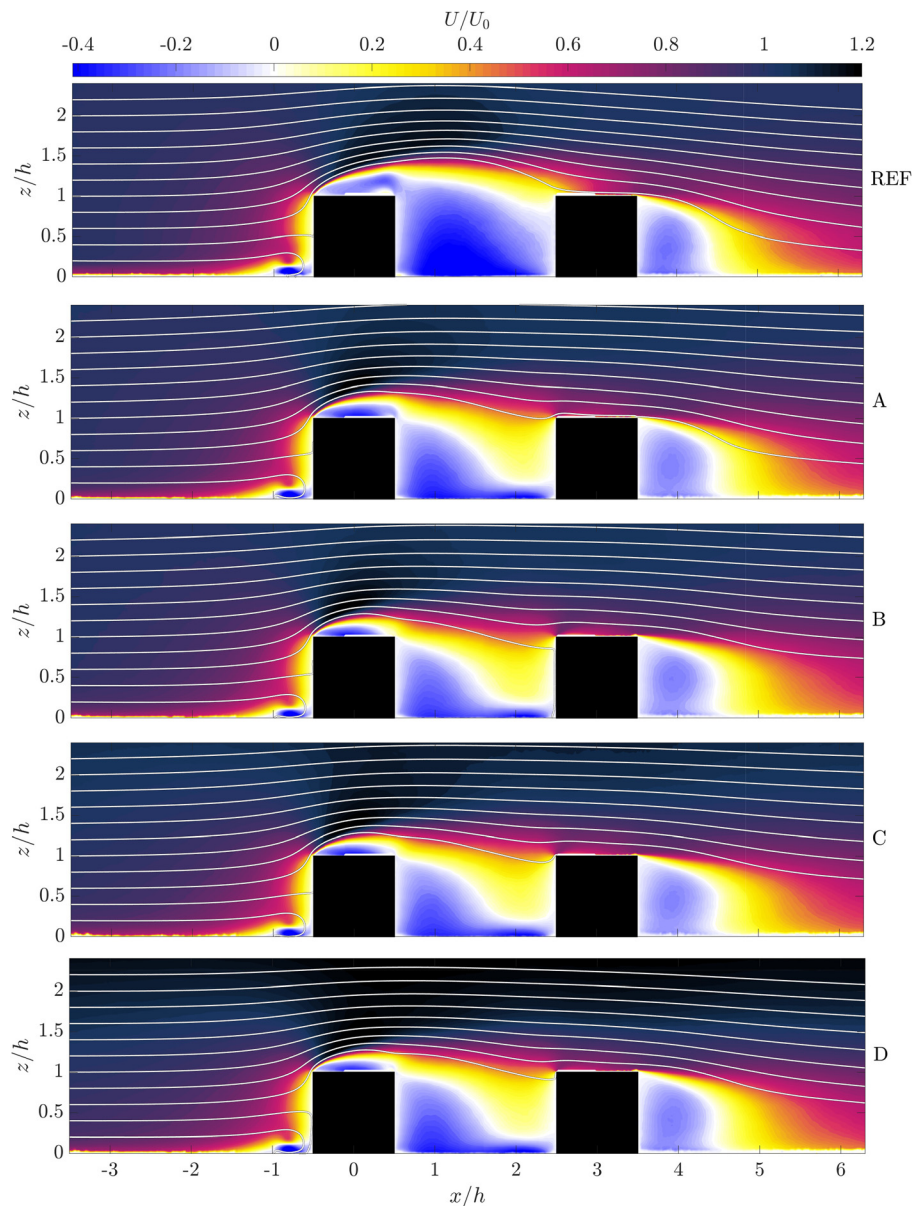**FIG. 5.** Spectral distribution of energy of the inflow cases.

FIG. 6. Streamwise velocity fields without the turbine present.

though. Note, that U_0 is different from U_∞, which was used to characterize the inflow without the cubes present. Figure 6 shows the U/U_0 fields with streamlines superimposed. Generally, the flow is slowed down by the presence of the upstream cube. At the windward bottom edge, a horseshoe vortex forms,[44] visible in the flow field as a small area of recirculating flow. At the windward top edge of the upstream cube, the flow separates for all inflow conditions. The streamlines are deflected upwards and a region of velocity surplus forms above the recirculation zone, leading to the development of a strong shear layer. In between the two cubes, a large region of recirculating flow evolves. Likewise, downstream of the second cube, the flow detaches and a region of slightly weaker recirculating flow is visible. The observations for REF are in agreement with Jooss *et al.*[18]

To evaluate the influence of turbulence intensity in the inflow, cases REF, A, and B are compared. It is apparent that the size of the recirculation zone on top of the upstream cube is significantly influenced by the different levels of u'_∞/U_∞. REF shows the largest region of reverse flow, extending past the leeward edge of the first cube and merging with the recirculating flow downstream of the cube. This is reduced for case A, where the recirculation zone approximately ends at the leeward edge, and even further for case B, where the two regions of reverse flow appear distinctly separated. Even more relevant potentially for the placement of a wind turbine is the extent of this recirculation zone in the vertical direction above the roof. The same trend is observed with decreasing size for increasing inflow turbulence intensity. These results are in agreement with observations made on a single

cube by Hearst *et al.*[46] for $0.5\% \leqslant u'_\infty/U_\infty \leqslant 8.9\%$. Similar to the present study, the turbulence was generated upstream with an active grid. Above the recirculation zone, the streamlines are deflected upwards and the flow accelerates. A region of accelerated flow is present for all cases, though its position and extent vary between the cases. Increasing u'_∞/U_∞ moves the start of this region upstream but limits its downstream extent. The recirculation zone in between the cubes is also strongly affected, the size of which decreases with increasing inflow turbulence intensity. As a result of this, the deflection of the streamlines is also reduced with increasing u'_∞/U_∞. This leads to different flow patterns on the downstream cube. While for REF, the flow reattaches mainly on top of the cube, for cases A and B, the reattachment point is moved so far upstream, that the flow instead impinges partly on the windward edge of the downstream cube. This leads to a reoccurrance, although substantially weakened, of flow separation at the windward top edge of cube 2, most apparent for case B. This changes the evolution of the flow on top of the downstream cube. For REF, it is dominated by a recovering wake from the upstream cube, whereas for case A, and even more so for case B, the flow is governed by the interaction between said wake and the newly separated flow on top of cube 2. The recirculation zone downstream of the second cube is not significantly affected by the change in u'_∞/U_∞ in the inflow.

For cases C and D, the vertical shear is visible upstream of the cubes with higher velocities at the top and lower velocities at the bottom. The velocity remains high in the top part of the field of view, whereas the lower region is disturbed by the presence of the cubes. The streamlines suggest that low momentum fluid from the bottom is transported up and above the cubes due to their blockage. Cases C and D are to be compared with the uniform velocity case B, which has a similar inflow turbulence intensity. It has to be noted though that the turbulence intensities for both cases C and D, at $u'_\infty/U_\infty = 10.4\%$ and $u'_\infty/U_\infty = 10.2\%$, respectively, fall slightly below case B at $u'_\infty/U_\infty = 11.5\%$. The recirculation zone on top of the upstream cube for C and D is significantly smaller than for case A, but it is still visibly larger than for case B, which suggests that even a 1.1% difference in turbulence intensity is significant for this flow. Cases C and D appear qualitatively similar, indicating that the different levels of shear examined here only have limited influence on the evolving flow patterns in this configuration. Thus, in the following, case C will be considered as a representative shear case in the proceeding analysis. Again, these findings are in agreement with findings on a single cube,[46] where both the stagnation point upstream of the cube and the reattachment length downstream were found to be independent of the examined incoming velocity profiles.

Generally, the flow field is dominated by the flow separation on the upstream leading edge of the first building. This suggests, that parameters, such as streamwise length of the upstream building and distance between the two buildings are of secondary importance to the flow above the roof. The extent of the flow separation is influenced by the upstream flow conditions, as outlined above, primarily by the level of freestream turbulence. Thus, considering the inflow conditions, it is
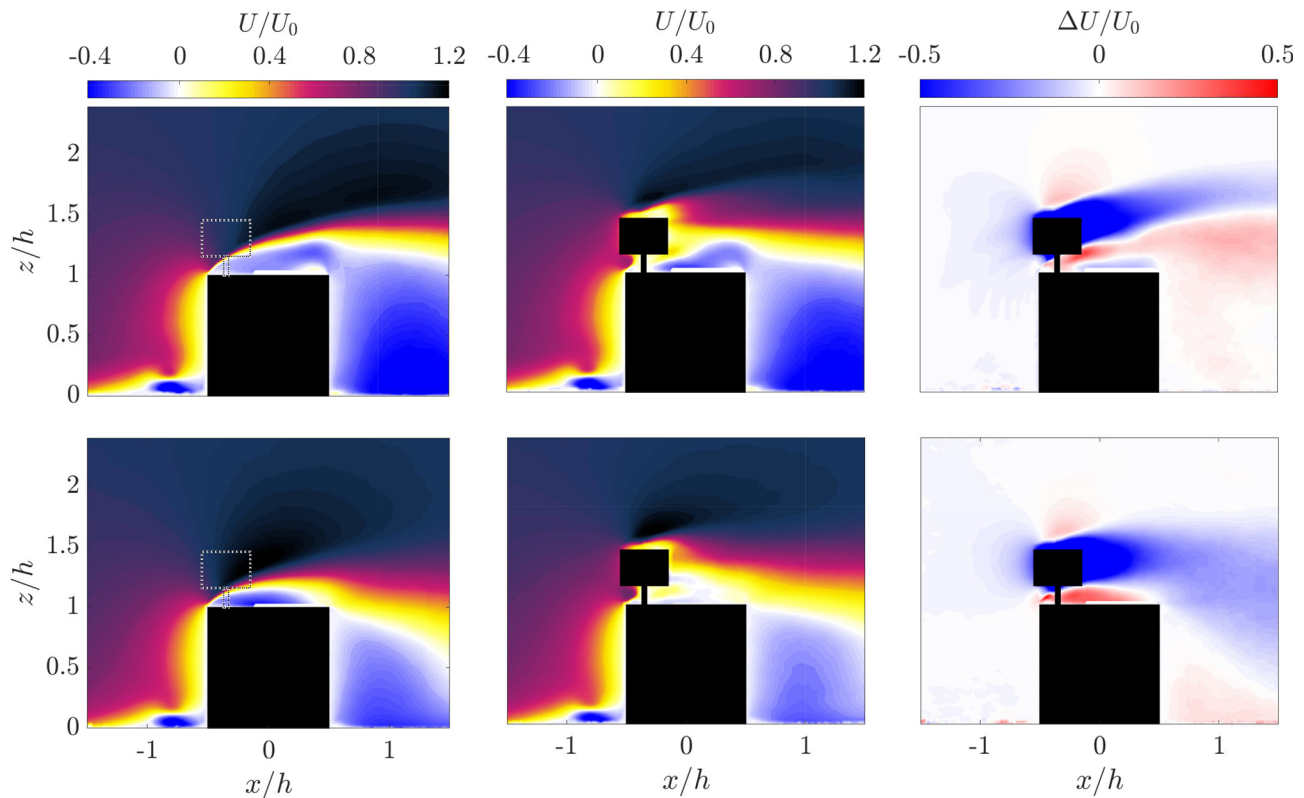

FIG. 7. Differential velocity fields at position H1 for case REF (top) and case B (bottom).

possible to assess the wind resources above building(s) based on the distance from the upstream edge.

C. Influence of the turbine on the flow

It is important to note that while the characterization of the flow field is a required prerequisite, it is not sufficient for evaluating the potential placement of a roof-mounted wind turbine. To capture the full scope of the problem, the turbine needs to be included in the analysis. Jooss *et al.*[18] demonstrated that the turbine has a significant influence on the flow field, and thus, on the available power P_a for a low turbulence intensity, uniform velocity inflow case, equivalent to case REF in this study. This influence is evaluated here for varying inflow conditions. Fundamentally, a wind turbine induces an upstream blockage effect.[19] This general behavior is observed for all cases at positions 1, 4, 5, and 6 for both low and high turbine, whereas at positions 2 and 3, a different behavior is detected. The two different effects are illustrated for cases REF and B at H1 in Fig. 7 and at L3 in Fig. 8. The figures display, from left to right, the flow field without the turbine, the flow field with the turbine, and the difference between the two $\Delta U/U_0$. A negative $\Delta U/U_0$ indicates a velocity deficit caused by the turbine, whereas a positive $\Delta U/U_0$ represents a velocity surplus in the presence of the turbine. At H1, for case REF, the turbine is placed upstream of the region of significant flow acceleration, whereas for case B, the flow accelerates approximately at $x/h = -0.35$, where the turbine is positioned. This results in a higher velocity for case B

compared to case REF without the turbine in place at H1, displayed by the dashed profiles in Fig. 9. Nevertheless, the turbine causes a decrease in the velocity immediately upstream of the turbine in both cases. The turbine still experiences higher velocity for case B compared to case REF. Figure 9 shows that the shape of the velocity profiles is also altered by the presence of the turbine at H1. It becomes more homogeneous between the bottom and the top half, but shows a velocity deficit in the center, where the blockage effect is the strongest. At position 2, not explicitly displayed here, the flow is governed by the recirculation zone (see Fig. 6). In high velocity regions, the turbine causes a decrease in the velocity similarly to position 1, whereas in low velocity regions close to the roof, the velocity is increased in the presence of the turbine. This behavior has also been observed by Jooss *et al.*[18]

At position 3, the recirculation zone continues to grow for case REF, while it decreases in size for cases A–C (see Fig. 6). Interestingly, this leads to diverging trends for the influence of the turbine on the flow field. While the velocity for case REF is increased throughout L3 and for most of H3 as well, the opposite is observed for cases B and C (not displayed here). Thus, the spread between case REF and cases B and C is reduced by the presence of the turbine here. Case A (not displayed here) falls somewhere in between, following the behavior of case REF at the bottom, and cases B and C higher up. The flow dynamics leading to this effect at L3 are shown for cases REF and B, with extracts of the respective flow fields in Fig. 8, and the corresponding velocity profiles in Fig. 9. For case REF at L3, the turbine is placed
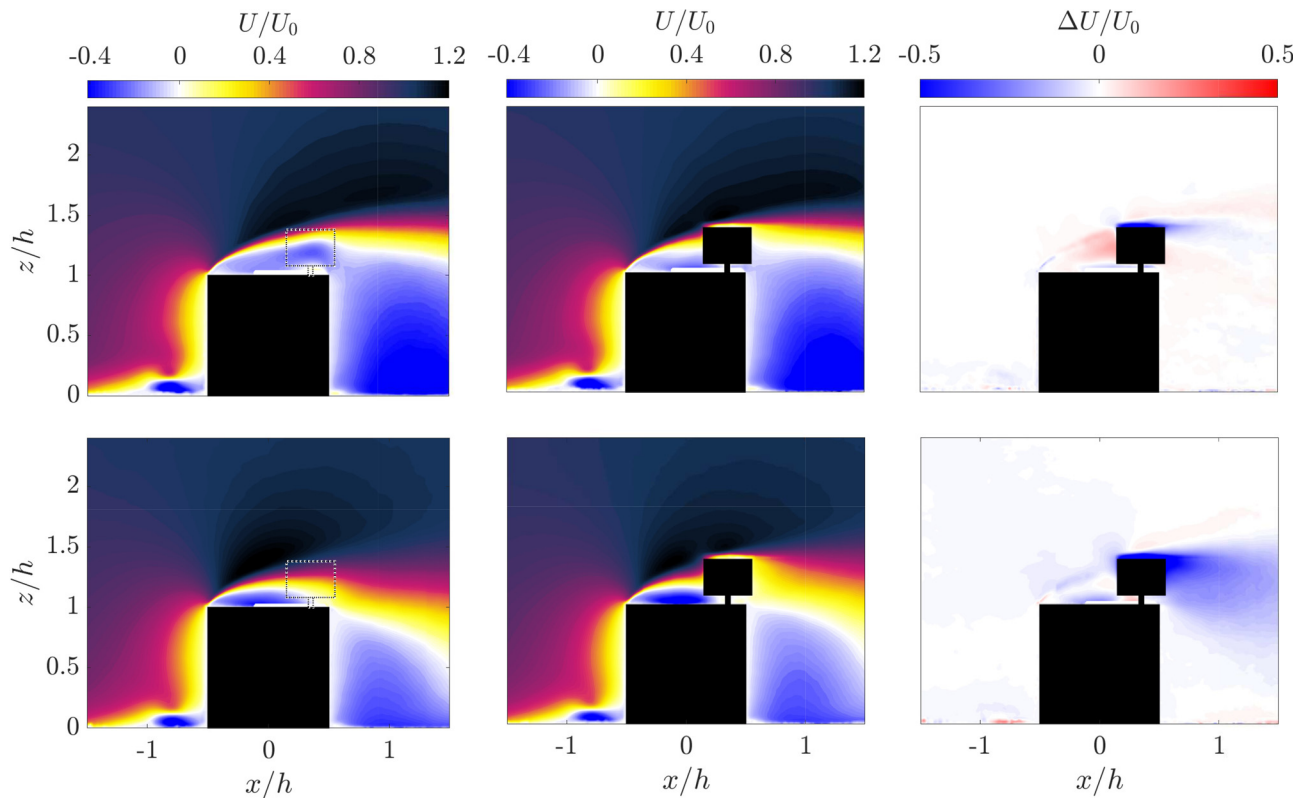

FIG. 8. Differential velocity fields at position L3 for case REF (top) and case B (bottom).
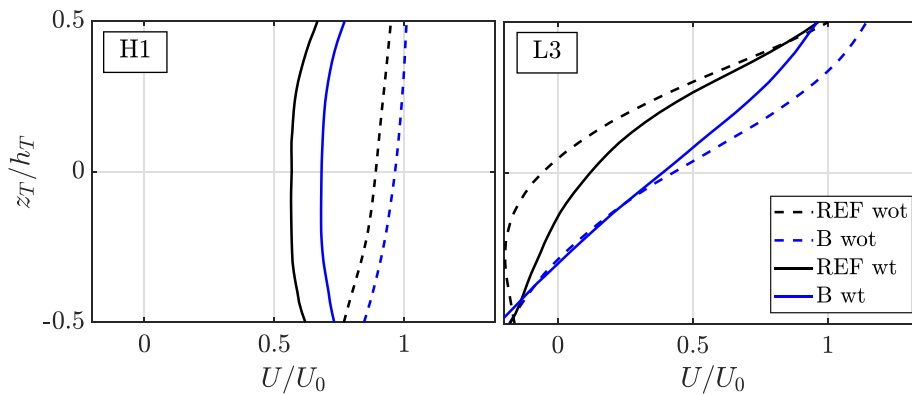
FIG. 9. Inflow profiles for cases REF and B with the turbine (solid lines) and without (dashed lines) at positions H1 and L3. Note that this is displayed in the frame of reference of the turbine, with $z_T = 0$ at the center of the turbine blades, and normalized by the turbine blade height h_T.

mainly in the recirculation zone. In the presence of the turbine, the recirculating flow is partly suppressed and a velocity surplus results along the rotor area. For case B, the recirculation zone is considerably smaller, and thus, the turbine is placed largely outside of it at L3. The size remains approximately unchanged with a slightly increased intensity in the presence of the turbine. The main influence of the turbine here is a velocity reduction in the top half, where high velocities are present initially. This example underlines how complex the interaction of the flow with the turbine can be. Not only is it dependent on the turbine's position,[18] but also on the inflow conditions, which here leads to contrasting implications caused by the turbine, even for the same position.

IV. ENERGY EXTRACTION

A. Power measurements

To evaluate the performance of the wind turbine in the varying inflow conditions at different positions on the roof, the power coefficient $C_P = \frac{P_m}{\frac{1}{2}A\rho U_0^3}$ is assessed. C_P is based on the mechanical power P_m of the turbine, which consists of the measured converted power P_c plus an estimate of the friction losses P_f. To enable a direct comparison of the power output between the different positions, U_0 far upstream of the cubes is used as a reference velocity for all positions. The focus of this study was not to evaluate how well the wind turbine itself performs but rather to compare different wind conditions (i.e., turbulence intensities and velocity shear) and turbine positions, and thus using the same velocity for all positions reflects a normalization whereby the power is the dominant parameter. The tip speed ratio $\lambda = \frac{\Omega_T r_T}{U_0}$, given by the ratio between the tip speed of the turbine blade and the flow velocity, is varied for every case to acquire full C_P-curves. These are displayed position by position in Fig. 10. To avoid clutter, only case C is displayed for the sheared inflow cases. The low turbine performs best at L1 for all cases. At L2, a similar power output is recorded, reduced by 9% on average. This reduction is more drastic for L3, where, on average, the C_P values measured 62% lower compared to L1. On the downstream cube, a gradual power increase is observed with increasing streamwise position. The spread between all positions is considerably smaller than on the upstream cube, with 10% between the highest average C_P at L6 and the lowest at L4. The trends between the positions are similar for the high turbine. The best overall performance is recorded at H1 and H2 with an average $C_{P\text{max}}$ of 0.058. Savonius turbines generally record lower C_P values than HAWTs and lift driven

VAWTs.[47,48] In addition, there is a Reynolds number dependence,[48] explaining the relatively low C_P values recorded in this study (see also Jooss et al.[18]). The reduction to position 3 is smaller for the high turbine compared to the low turbine, but still significant at 24% on average. For the downstream cube, only small differences between the three positions are recorded, with an 8% difference in the average $C_{P\text{max}}$ between H6 (the most favorable of the three) and H4 (the least favorable).

Comparing the different inflow cases, it is observed that inflow turbulence intensity impacts the turbine performance significantly, showing in the discrepancy between case REF and all other cases. Also case B is different from case A at almost every position. The influence of shear is less clear with case C collapsing with case B for most of the positions, with slight advantages at position 3. Figure 11 illustrates the relation of $C_{P\text{max}}$ with u'_∞/U_∞ and $\Delta U(z)/U_\infty$ explicitly for all examined positions. The influence of the turbulence intensity is apparent, with higher u'_∞/U_∞ leading to higher $C_{P\text{max}}$ generally. The trend flattens on average with increasing u'_∞/U_∞. The influence is greater for the low turbine position, with an average increase in 44% from case REF to case B, compared to 28% for the high turbine. On the upstream cube, this is caused by the reduced size of the recirculation zone for high u'_∞/U_∞ as illustrated in Fig. 6. A larger part of the turbine is placed outside of the chaotic low momentum flow, and more of the accelerated flow above is captured and utilized. In addition, the region of accelerated flow is intensified in the presence of high u'_∞/U_∞. On the downstream cube, the differences stem from an accelerated recovery of the wake of the upstream cube with increasing turbulence intensity in the inflow. Mixing is enhanced, and thus, more of the higher momentum fluid from the top is entrained, leading to higher velocities on top of the downstream cube. This effect is further enhanced by the fact that the flow is less deflected above the upstream cube, thus creating a smaller wake region initially. For shear, there is no clear trend, with a 4% average increase for the low and a 1% average increase for the high turbine from case B to case D. The streamlines in Fig. 6 show the transport of low momentum fluid from the bottom to above the cubes. In addition, the slight difference in u'_∞/U_∞ causes a small velocity deficit originating from the trailing edge of the cube. This appears to balance out the higher momentum fluid higher up. Overall, the shear takes a backseat compared to turbulence intensity in this configuration, not only for the impact on the flow field, but also for the impact on the power output of the turbine.
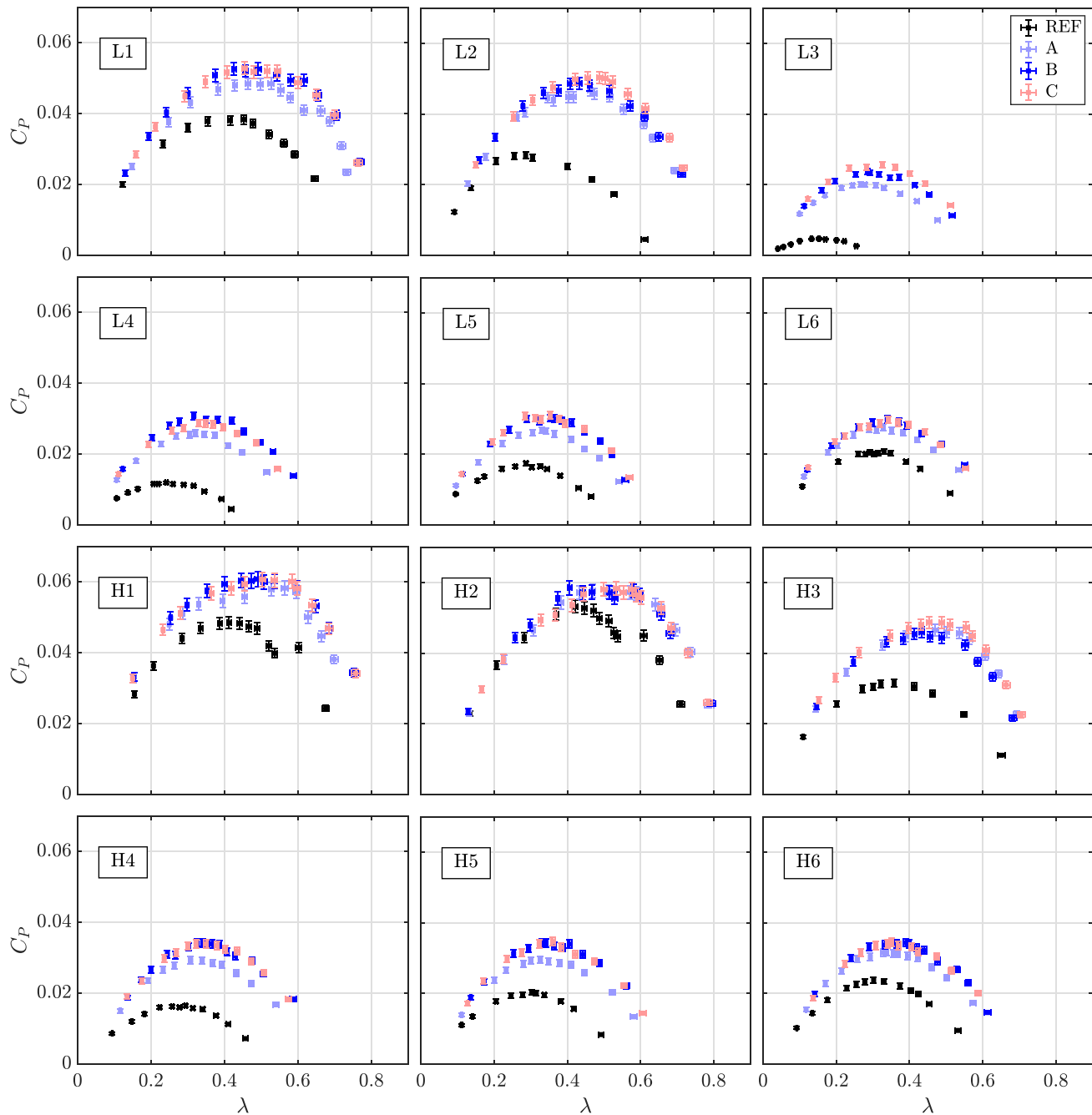
FIG. 10. C_P-curves for the different inflow cases at all positions and heights.

To illustrate the trends for the individual inflow cases, Fig. 12 displays $C_{P\max}$ relative to the position of the turbine. For the low turbine, the trends are similar between all cases. The reduction from position 1 to position 2 is more significant for case REF than for the other three cases. On the second cube, case B shows close to no evolution. With decreasing u'_∞/U_∞, the change from L4 to L6 becomes increasingly

significant. Case C only shows small differences from case B, with slightly higher $C_{P\max}$ at L3 and slightly lower $C_{P\max}$ at L4. The same is observed for the high turbine with a perfect collapse of cases B and C, except at H3, where case C has a minor advantage. While cases B and C show a decreasing power output from H1 to H2, case A remains approximately constant and case REF even shows an increase in

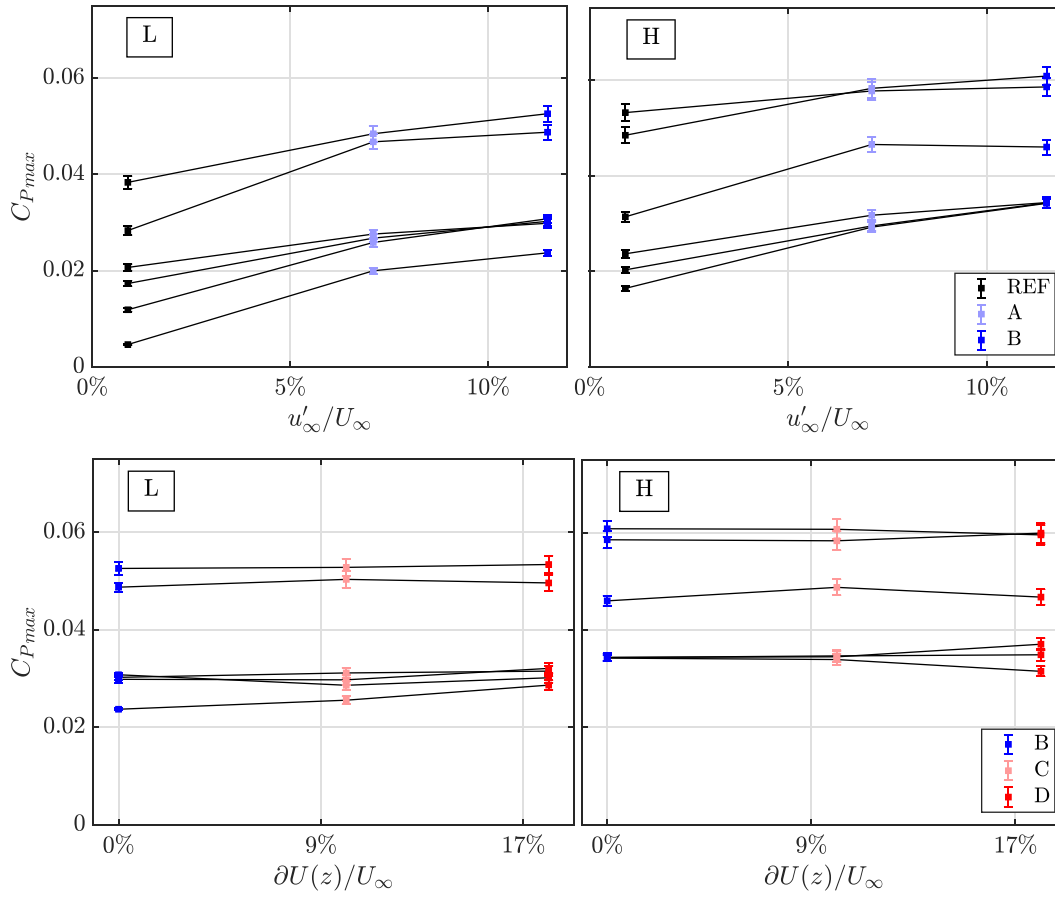**FIG. 11.** Relation of $C_{P\text{max}}$ to turbulence intensity and shear. Each line represents one turbine position.
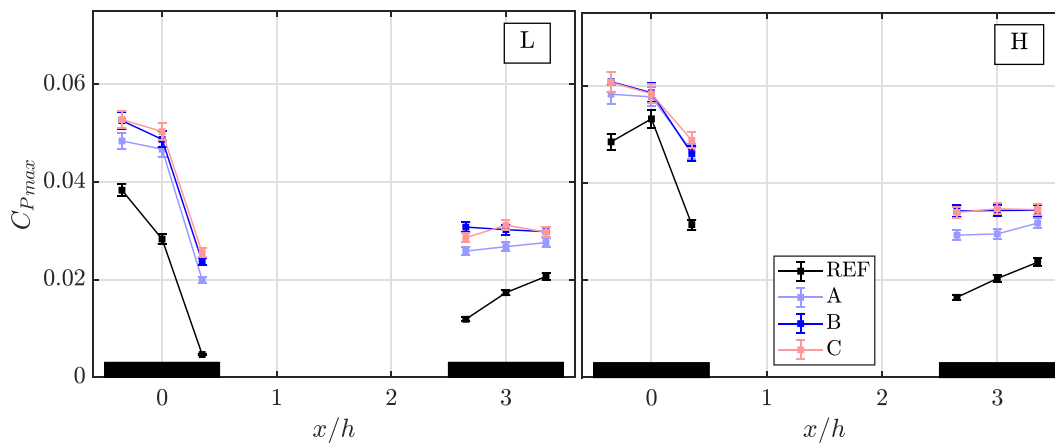

FIG. 12. Evolution of $C_{P\text{max}}$ through the different positions for the various inflow cases. The lines between the positions are shown to visualize the trends for the individual cases throughout the turbine positions. Note that the trends are not necessarily linear between measurement positions.

$C_{P\text{max}}$. This can be explained by the upstream shift of the acceleration region for increasing u'_∞/U_∞. This benefits the power output at H1 compared to H2 for the more turbulent cases. On the second cube, similar to the low turbine, there is close to no change for cases B and C, whereas case A and even more case REF increase their performance from position 4 to position 6.

B. Analysis of individual positions

In this section, certain interesting positions are examined in more detail. At L3, the C_P-curves show differences between all four displayed inflow cases (see Fig. 10). Case C yields the highest power output, followed by cases B and A, and with a large gap, case REF. To understand the dynamics behind this, the flow the turbine experiences here is presented in Fig. 13. The recirculation zone is significantly smaller for case A compared to REF, which leads to the turbine experiencing higher velocities. This is reflected in the velocity profiles immediately upstream ($-0.02h$) of the turbine. Case A shows slightly higher velocities compared to case B, which suggests a stronger flow acceleration. However, in the lower area, the recirculation zone is diminished further for case B, which yields higher velocities in the lower rotor area. This compensates for the slight deficit at the top and leads to a higher average velocity for case B compared to case A, which results in a higher power output as well. Comparing case C to case B shows a more pronounced acceleration upstream of the upper part of the turbine. This results in a steeper velocity gradient, yielding higher velocities along the entire rotor swept area.

At L4 (Fig. 14), the turbine is positioned in a recovering wake from the upstream cube. The difference between case REF and case A is apparent from the flow field. The wake is less recovered for REF, resulting in lower momentum flow upstream of the turbine, and thus, lower C_P. This trend continues with increasing u'_∞/U_∞. Increased mixing with the higher momentum fluid from the top yields even higher velocities for case B, resulting in an increased power output. The flow field for case C shows high velocities above the turbine; however, upstream of the rotor swept area, the velocities are very similar to case B. Slightly higher velocities at the top are balanced by slightly lower velocities at the bottom, yielding close to identical C_P-curves. Figure 6 suggests that the slightly higher u'_∞/U_∞ of case B compared to case C leads to an increased curvature of the streamlines downstream of cube 1, bringing higher momentum flow down closer to the roof. This appears to compensate for the difference in shear between the two cases, underlining the dominant role of turbulence intensity compared to shear in this configuration.

H3 (Fig. 15) presents an interesting scenario, as this is the one position where case A yields a higher $C_{P\text{max}}$ than case B. As described in Sec. III B, u'_∞/U_∞ does not only affect the recirculation zone on top of the upstream cube, but also the region of accelerated flow above. While the acceleration is enhanced by high u'_∞/U_∞, it extends farthest for the low turbulence case REF. This is visible in the flow fields and velocity profiles at H3, where REF shows the most pronounced acceleration, followed by case A. For case REF, the low velocity region extends farther up from the roof than for the other cases, leading to significantly lower velocities in the lower half of the turbine swept area,

FIG. 13. Analysis velocity fields at position L3. From top left to right case REF, case A, case B, and case C, with the velocity profiles 0.02h upstream of the turbine at the bottom. Note that this is displayed in the frame of reference of the turbine, with $z_T = 0$ at the center of the turbine blades, and normalized by the turbine blade height h_T.
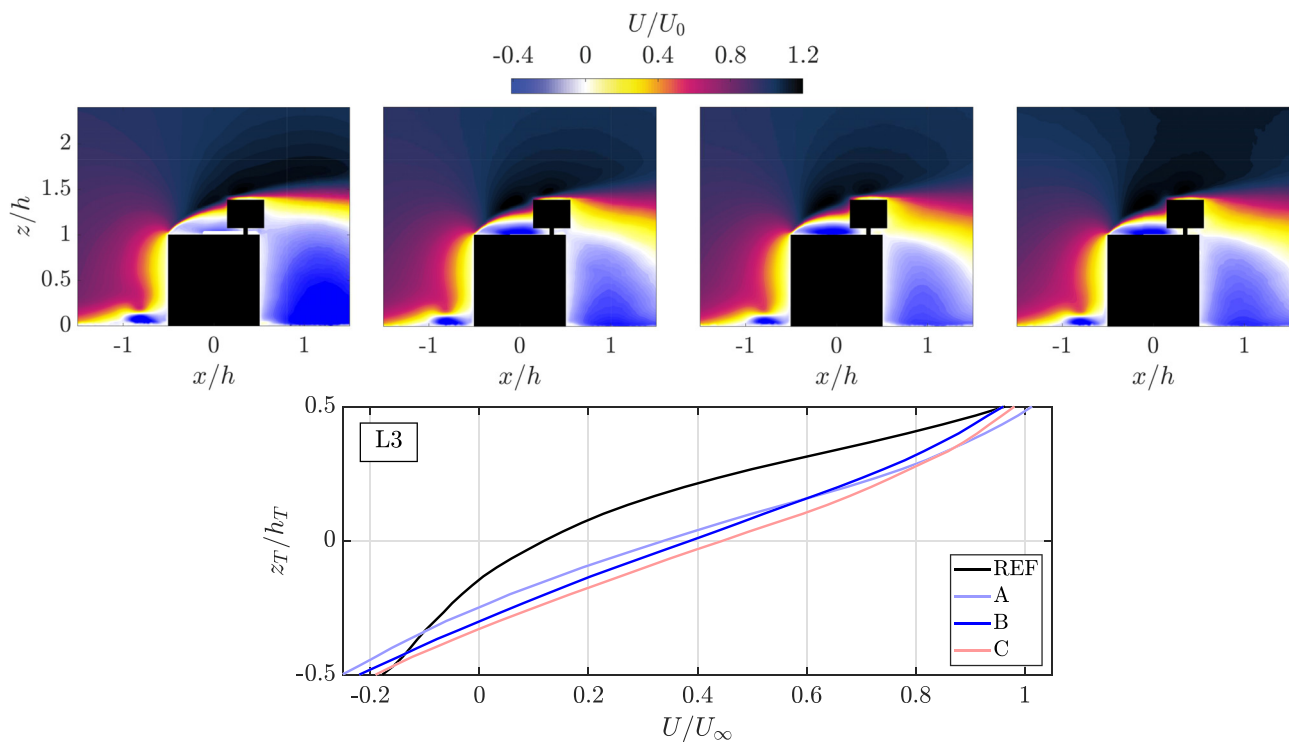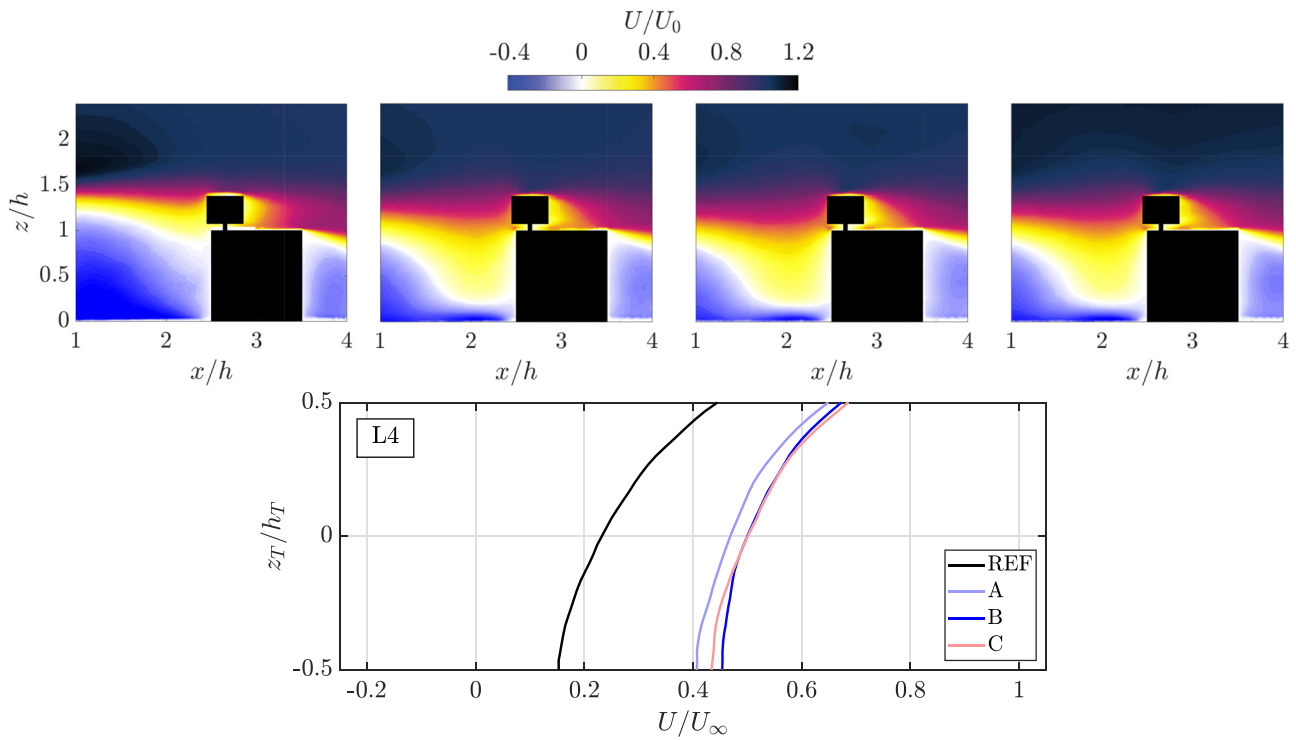
FIG. 14. Analysis velocity fields at position L4. From top left to right case REF, case A, case B, and case C, with the velocity profiles 0.02h upstream of the turbine at the bottom. Note that this is displayed in the frame of reference of the turbine, with $z_T = 0$ at the center of the turbine blades, and normalized by the turbine blade height h_T.

FIG. 15. Analysis at position H3. From top left to right case REF, case A, case B, and case C, with the velocity profiles 0.02h upstream of the turbine at the bottom. Note that this is displayed in the frame of reference of the turbine, with $z_T = 0$ at the center of the turbine blades, and normalized by the turbine blade height h_T.
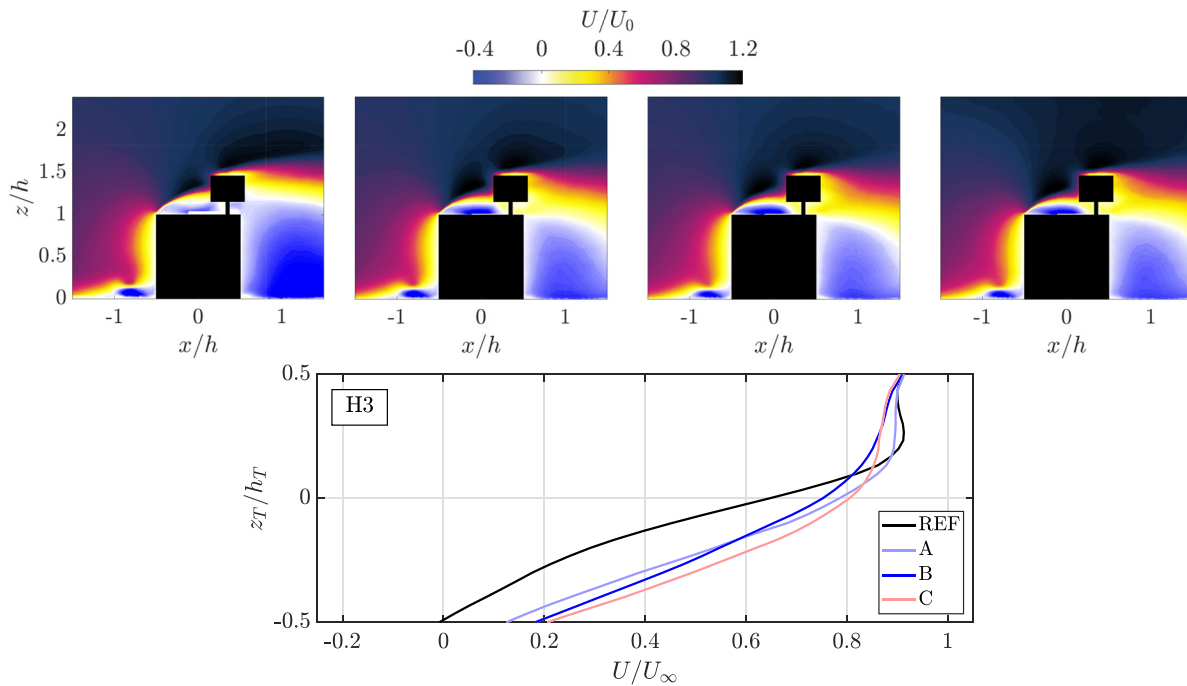
and thus, overall lower power output. Case A only shows slightly lower velocities in the lowest part of the turbine compared to case B. This is overcompensated by the increased acceleration in the upper half, yielding a higher power output for case A compared to case B. Case C also outperforms B at H3. Similar to L3, the high velocity region above the turbine caused by the shear for case C produces a stronger velocity gradient, leading to higher velocities throughout most parts of the turbine.

The results at L4 are representative for the general trends at most positions. Cases B and C with the highest inflow u'_∞/U_∞ yielded the highest power output. C_P was slightly reduced for case A and significantly reduced for case REF. At L3, case C slightly outperforms case B, again followed by case A and case REF. Similar, at position H3, the turbine extracts slightly more power for the sheared inflow case C. However, H3 is unique, as it is the only position, where case A yields a higher power output than case B.

In general, a high turbine position is beneficial, most notably on a building relatively unaffected by its surroundings (the upstream cube in this study). This effect is diminished for a building in the wake of another building (the downstream cube in this study). For realistically high turbulence intensities, a placement close to the wind facing side of the building promises the highest power output. A central position generally yields an only slightly reduced power output and is thus a highly suitable option for the placement of a roof-mounted wind turbine, in particular when the prevailing wind direction is unclear or strongly varying. This is especially relevant for a relatively unobstructed building as the reduction toward the leeward side of the building in that case is significant. In combination with wind data from local weather stations, this can be a starting point to decide on the position of a roof-mounted wind turbine. This should be complemented with wind velocity measurements at the desired position to ensure reasonable power output.

V. CONCLUSIONS

The impact of varying flow conditions, a characteristic for the urban environment, on the flow field and performance of a roof-mounted vertical axis wind turbine has been investigated. A Savonius (drag) type vertical axis wind turbine was mounted at six streamwise positions at two heights on top of two cubes, representing model buildings, in a wind tunnel. The flow field was captured with particle image velocimetry along the center plane, and the converted power of the turbine was measured with a small generator and an optical sensor. The turbulence intensity and shear in the inflow were varied with an active grid, yielding a total of five inflow conditions with $0.9\% \leqslant u'_\infty/U_\infty \leqslant 11.5\%$ and $0\% \leqslant \Delta U(z)/U_\infty \leqslant 17\%$.

It was found that increasing u'_∞/U_∞ leads to a suppression of the recirculation zone on top of the upstream cube. This is in agreement with the findings on a single cube.[46] Above the recirculating flow, a region of accelerated flow arises. This region moves upstream for increasing u'_∞/U_∞. The recirculation zone in between the cubes is also drastically reduced in size for higher levels of u'_∞/U_∞. The smaller recirculation zones lead to less deflection of the streamlines. Together with enhanced mixing, this alters the reattachment of the flow on the downstream cube. For low u'_∞/U_∞, the flow primarily reattaches on top of the downstream cube, whereas for high u'_∞/U_∞, it impinges on the windward face of the second cube and leads to slight re-separation of the flow. The impact of shear on the flow phenomenology around the two model buildings is less prominent. The high velocity region

high above the roof does not interact very much with the flow immediately above the roof. Low momentum fluid from the bottom is transported up above the cubes through the deflection of the streamlines caused by the presence of the cubes.

The turbine itself affects the flow field significantly, in agreement with Jooss et al.[18] This interaction is complex and highly dependent on the turbine position and the local flow. Furthermore, it was shown in this study that even for the identical turbine position, the impact can vary substantially dependent on the inflow conditions. This underlines the importance of including the turbine in such an analysis.

The power measurements show that between the two examined turbine heights, the high position yielded higher C_P values independent of the streamwise position. The difference between low and high position is largest at position 3. Here, the high turbine is largely outside the recirculation zone, whereas the low turbine primarily experiences low velocities caused by the separated flow. Overall, positions 1 and 2 with the high turbine yielded the highest average power output.

Most notably, it was demonstrated that the influence of u'_∞/U_∞ is dominant on this problem compared to $\Delta U(z)/U_\infty$, for the examined levels of u'_∞/U_∞ and $\Delta U(z)/U_\infty$ here. Similar power coefficients were recorded for the various levels of $\Delta U(z)/U_\infty$, with no apparent trend. Increasing levels of u'_∞/U_∞, on the other hand, led to increasing power output throughout most turbine positions. The influence was found to be larger for turbine positions close to the roof, and also more significant for the upstream cube generally. For increasing u'_∞/U_∞, the trend of increasing C_P flattens out, indicating that this elevated potential is limited.

AUTHOR DECLARATIONS
Conflict of Interest

The authors have no conflicts to disclose.

Author Contributions

Yannick Jooss: Conceptualization (equal); Formal analysis (lead); Investigation (lead); Methodology (lead); Visualization (lead); Writing – original draft (lead); Writing – review & editing (equal). **R. Jason Hearst:** Conceptualization (lead); Formal analysis (supporting); Investigation (supporting); Methodology (equal); Resources (equal); Supervision (equal); Visualization (supporting); Writing – review & editing (equal). **Tania Bracchi:** Conceptualization (equal); Formal analysis (supporting); Funding acquisition (equal); Investigation (supporting); Methodology (supporting); Resources (equal); Supervision (equal); Visualization (supporting); Writing – review & editing (equal).

DATA AVAILABILITY

The data that support the findings of this study are available from the corresponding author upon reasonable request.

REFERENCES

[1]United Nations, "Transforming our world: The 2030 agenda for sustainable development," Resolution 70/1 (21 October 2015).

[2]A. Kc, J. Whale, and T. Urmee, "Urban wind conditions and small wind turbines in the built environment: A review," Renewable Energy **131**, 268–283 (2019).

[3]J. T. Millward–Hopkins, A. S. Tomlin, L. Ma, D. Ingham, and M. Pourkashanian, "The predictability of above roof wind resource in the urban roughness sublayer," Wind Energy **15**, 225–243 (2012).

[4]T. R. Oke, "The distinction between canopy and boundary–layer urban heat islands," Atmosphere **14**, 268–277 (1976).

[5]T. Oke, "The urban energy balance," Prog. Phys. Geogr. **12**, 471–508 (1988).

[6]L. Wang, D. Li, Z. Gao, T. Sun, X. Guo, and E. Bou-Zeid, "Turbulent transport of momentum and scalars above an urban canopy," Boundary-Layer Meteorol. **150**, 485–511 (2014).

[7]H. Cheng and I. P. Castro, "Near wall flow over urban-like roughness," Boundary-Layer Meteorol. **104**, 229–259 (2002).

[8]R. Wagner, I. Antoniou, S. M. Pedersen, M. S. Courtney, and H. E. Jùrgensen, "The influence of the wind speed profile on wind turbine performance measurements," Wind Energy **12**, 348–362 (2009).

[9]T. Mücke, D. Kleinhans, and J. Peinke, "Atmospheric turbulence and its influence on the alternating loads on wind turbines," Wind Energy **14**, 301–316 (2011).

[10]M. Roth, "Review of atmospheric turbulence over cities," Quart. J. R. Meteorol. Soc. **126**, 941–990 (2000).

[11]A. Choukulkar, Y. Pichugina, C. T. M. Clack, R. Calhoun, R. Banta, A. Brewer, and M. Hardesty, "A new formulation for rotor equivalent wind speed for wind resource assessment and wind power forecasting," Wind Energy **19**, 1439–1452 (2016).

[12]S. Mertens, "The energy yield of roof mounted wind turbines," Wind Eng. **27**, 507–518 (2003).

[13]L. Ledo, P. B. Kosasih, and P. Cooper, "Roof mounting site analysis for micro-wind turbines," Renewable Energy **36**, 1379–1391 (2011).

[14]I. Abohela, N. Hamza, and S. Dudek, "Effect of roof shape, wind direction, building height and urban configuration on the energy yield and positioning of roof mounted wind turbines," Renewable Energy **50**, 1106–1118 (2013).

[15]A. Al-Quraan, T. Stathopoulos, and P. Pillay, "Comparison of wind tunnel and on site measurements for urban wind energy estimation of potential yield," J. Wind Eng. Ind. Aerodyn. **158**, 1–10 (2016).

[16]A. Sarkic Glumac, H. Hemida, and R. Höffer, "Wind energy potential above a high-rise building influenced by neighboring buildings: An experimental investigation," J. Wind Eng. Ind. Aerodyn. **175**, 32–42 (2018).

[17]G. Vita, A. Sarkic Glumac, H. Hemida, S. Salvadori, and C. Baniotopoulos, "On the wind energy resource above high-rise buildings," Energies **13**, 3641 (2020).

[18]Y. Jooss, R. Bolis, T. Bracchi, and R. J. Hearst, "Flow field and performance of a vertical-axis wind turbine on model buildings," Flow **2**, E10 (2022).

[19]D. Medici, S. Ivanell, J.-A. Dahlberg, and P. H. Alfredsson, "The upstream flow of a wind turbine: Blockage effect," Wind Energy **14**, 691–697 (2011).

[20]S. Yan, S. Shi, X. Chen, X. Wang, L. Mao, and X. Liu, "Numerical simulations of flow interactions between steep hill terrain and large scale wind turbine," Energy **151**, 740–747 (2018).

[21]R. B. Cal, J. Lebrón, L. Castillo, H. S. Kang, and C. Meneveau, "Experimental study of the horizontally averaged flow structure in a model wind-turbine array boundary layer," J. Renewable Sustainable Energy **2**, 013106 (2010).

[22]J. Bartl, F. Pierella, and L. Saetrana, "Wake measurements behind an array of two model wind turbines," in Energy Procedia Selected Papers from Deep Sea Offshore Wind R&D Conference, Trondheim, Norway, 19–20 January 2012 (Elsevier, 2012), Vol. 24, pp. 305–312.

[23]C. L. Bottasso, F. Campagnolo, and V. Petrović, "Wind tunnel testing of scaled wind turbine models: Beyond aerodynamics," J. Wind Eng. Ind. Aerodyn. **127**, 11–28 (2014).

[24]J. Schottler, A. Hölling, J. Peinke, and M. Hölling, "Design and implementation of a controllable model wind turbine for experimental studies," J. Phys. **753**, 072030 (2016).

[25]M. Bastankhah and F. Porté-Agel, "Experimental and theoretical study of wind turbine wakes in yawed conditions," J. Fluid Mech. **806**, 506–541 (2016).

[26]I. Neunaber, M. Hölling, R. J. A. M. Stevens, G. Schepers, and J. Peinke, "Distinct turbulent regions in the wake of a wind turbine and their inflow-dependent locations: The creation of a wake map," Energies **13**, 5392 (2020).

[27]L. Li, R. J. Hearst, M. A. Ferreira, and B. Ganapathisubramani, "The near-field of a lab-scale wind turbine in tailored turbulent shear flows," Renewable Energy **149**, 735–748 (2020).

[28]A. Segalini and J.-A. Dahlberg, "Blockage effects in wind farms," Wind Energy **23**, 120–128 (2020).

[29]S. d J. Helvig, M. K. Vinnes, A. Segalini, N. A. Worth, and R. J. Hearst, "A comparison of lab-scale free rotating wind turbines and actuator disks," J. Wind Eng. Ind. Aerodyn. **209**, 104485 (2021).

[30]S. Gambuzza and B. Ganapathisubramani, "The effects of free-stream turbulence on the performance of a model wind turbine," J. Renewable Sustainable Energy **13**, 023304 (2021).

[31]C. J. Simão Ferreira, G. J. W. van Bussel, and G. A. M. van Kuik, "Wind tunnel hotwire measurements, flow visualization and thrust measurement of a VAWT in skew," J. Sol. Energy Eng. **128**, 487–497 (2006).

[32]C. Simão Ferreira, G. van Kuik, G. van Bussel, and F. Scarano, "Visualization by PIV of dynamic stall on a vertical axis wind turbine," Exp. Fluids **46**, 97–108 (2009).

[33]J. O. Dabiri, "Potential order-of-magnitude enhancement of wind farm power density via counter-rotating vertical-axis wind turbine arrays," J. Renewable Sustainable Energy **3**, 043104 (2011).

[34]S. Shamsoddin and F. Porté-Agel, "Large eddy simulation of vertical axis wind turbine wakes," Energies **7**, 890–912 (2014).

[35]I. Hui, B. E. Cain, and J. O. Dabiri, "Public receptiveness of vertical axis wind turbines," Energy Policy **112**, 258–271 (2018).

[36]M. A. Miller, S. Duvvuri, I. Brownstein, M. Lee, J. O. Dabiri, and M. Hultmark, "Vertical-axis wind turbine experiments at full dynamic similarity," J. Fluid Mech. **844**, 707–720 (2018).

[37]M. M. Aslam Bhutta, N. Hayat, A. U. Farooq, Z. Ali, S. R. Jamil, and Z. Hussain, "Vertical axis wind turbine – A review of various configurations and design techniques," Renewable Sustainable Energy Rev. **16**, 1926–1939 (2012).

[38]S. Kooiman and S. Tullis, "Response of a vertical axis wind turbine to time varying wind conditions found within the urban environment," Wind Eng. **34**, 389–401 (2010).

[39]D. Li, S. Wang, and P. Yuan, "A review of micro wind turbines in the built environment," in 2010 Asia-Pacific Power and Energy Engineering Conference (IEEE, 2010), pp. 1–4.

[40]L. C. Pagnini, M. Burlando, and M. P. Repetto, "Experimental power curve of small-size wind turbines in turbulent urban environment," Appl. Energy **154**, 112–121 (2015).

[41]M. Ge, D. F. Gayme, and C. Meneveau, "Large-eddy simulation of wind turbines immersed in the wake of a cube-shaped building," Renewable Energy **163**, 1063–1077 (2021).

[42]S. Zhang, B. Du, M. Ge, and Y. Zuo, "Study on the operation of small rooftop wind turbines and its effect on the wind environment in blocks," Renewable Energy **183**, 708–718 (2022).

[43]R. J. Martinuzzi and B. Havel, "Turbulent flow around two interfering surface-mounted cubic obstacles in tandem arrangement," J. Fluids Eng. **122**, 24 (2000).

[44]R. J. Martinuzzi and B. Havel, "Vortex shedding from two surface-mounted cubes in tandem," Int. J. Heat Fluid Flow **25**, 364–372 (2004).

[45]A. Yakhot, H. Liu, and N. Nikitin, "Turbulent flow around a wall-mounted cube: A direct numerical simulation," Int. J. Heat Fluid Flow **27**, 994–1009 (2006).

[46]R. J. Hearst, G. Gomit, and B. Ganapathisubramani, "Effect of turbulence on the wake of a wall-mounted cube," J. Fluid Mech. **804**, 513–530 (2016).

[47]A. J. Alexander and B. P. Holownia, "Wind tunnel tests on a savonius rotor," J. Wind Eng. Ind. Aerodyn. **3**, 343–351 (1978).

[48]J. V. Akwa, H. A. Vielmo, and A. P. Petry, "A review on the performance of savonius wind turbines," Renewable Sustainable Energy Rev. **16**, 3054–3064 (2012).

[49]J. Kumbernuss, J. Chen, H. X. Yang, and L. Lu, "Investigation into the relationship of the overlap ratio and shift angle of double stage three bladed vertical axis wind turbine (VAWT)," J. Wind Eng. Ind. Aerodyn. **107–108**, 57–75 (2012).

[50]M. Bastankhah and F. Porté-Agel, "A new miniature wind turbine for wind tunnel experiments. Part I: Design and performance," Energies **10**, 908 (2017).

[51]G. S. West and C. J. Apelt, "The effects of tunnel blockage and aspect ratio on the mean flow past a circular cylinder with Reynolds numbers between 104 and 105," J. Fluid Mech. **114**, 361–377 (1982).

[52]R. J. Hearst and P. Lavoie, "The effect of active grid initial conditions on high Reynolds number turbulence," Exp. Fluids **56**, 185 (2015).

[53]L. Mydlarski and Z. Warhaft, "On the onset of high-Reynolds-number grid-generated wind tunnel turbulence," J. Fluid Mech. **320**, 331–368 (1996).

[54]J. V. Larssen and W. J. Devenport, "On the generation of large-scale homogeneous turbulence," Exp. Fluids **50**, 1207–1223 (2011).

09 November 2023 09:46:12

[55]R. J. Hearst and B. Ganapathisubramani, "Tailoring incoming shear and turbulence profiles for lab-scale wind turbines," Wind Energy **20**, 2021–2035 (2017).

[56]I. P. Castro and A. G. Robins, "The flow around a surface-mounted cube in uniform and turbulent streams," J. Fluid Mech. **79**, 307–335 (1977).

[57]K. Uehara, S. Wakamatsu, and R. Ooka, "Studies on critical Reynolds number indices for wind-tunnel experiments on flow within urban areas," Boundary-Layer Meteorol. **107**, 353–370 (2003).

[58]N. S. Sharp, S. Neuscamman, and Z. Warhaft, "Effects of large-scale free stream turbulence on a turbulent boundary layer," Phys. Fluids **21**, 095105 (2009).

[59]E. Dogan, R. J. Hearst, R. E. Hanson, and B. Ganapathisubramani, "Spatial characteristics of a zero-pressure-gradient turbulent boundary layer in the presence of free-stream turbulence," Phys. Rev. Fluids **4**, 084601 (2019).

[60]C. Vanderwel and S. Tavoularis, "Coherent structures in uniformly sheared turbulent flow," J. Fluid Mech. **689**, 434–464 (2011).

09 November 2023 09:46:12